This is an *Accepted Manuscript*, which has been through the Royal Society of Chemistry peer review process and has been accepted for publication.

Accepted Manuscripts are published online shortly after acceptance, before technical editing, formatting and proof reading. Using this free service, authors can make their results available to the community, in citable form, before we publish the edited article. We will replace this *Accepted Manuscript* with the edited and formatted *Advance Article* as soon as it is available.

You can find more information about *Accepted Manuscripts* in the **Information for Authors**.

The Intriguiging Question of Anionic Redox in High-Energy Density Cathodes for Li-ion Batteries

M. Saubanère[1,3], E. McCalla[1,3], J.-M. Tarascon[1,3] M.-L. Doublet[2,3]

[1] *Collège de France, Laboratoire de Chimie du Solide et Energie,*

11, Rue Marcelin Berthelot, 75005 Paris, France

[2] *Institut Charles Gerhardt, CNRS - Université Montpellier 2,*

Place Eugène Bataillon, 34095 Montpellier, France.

[3] *Réseau Français sur le Stockage Electrochimique*

de l'Energie - RS2E FR3459, Amiens, France

(Dated: October 29, 2015)

Abstract

The energy density delivered by a Li-ion battery is a key parameter that needs to be significantly increased to address the global question of energy storage for the next 40 years. This quantity is directly proportional to the battery voltage (V) and the battery capacity (C) which are difficult to improve simultaneously when materials exhibit a classical cationic redox activity. Recently, a cumulative cationic (M^{4+}/M^{5+}) and anionic ($2O^{2-}/(O_2)^{n-}$) redox activity has been demonstrated in the Li-rich Li_2MO_3 family of compounds, therefore enabling doubling the energy density with respect to high-potential cathodes such as transition metal phosphates and sulfates. This paper aims at clarifying the origin of this extra capacity by addressing some fundamental questions regarding reversible anionic redox in high-potential electrodes for Li-ion batteries. First, the ability of the system to stabilize the oxygen holes generated by Li-removal and to achieve a reversible oxo- to peroxo-like ($2O^{2-}/(O_2)^{n-}$) transformation is elucidated by means of a metal-driven reductive coupling mechanism. The penchant of the system for undergoing this reversible anionic redox or releasing O_2 gas is then discussed in regards to experimental results for $3d$- and $4d$-based Li_2MO_3 phases. Finally, robust indicators are built as tools to predict which materials in the Li-rich TM-oxides family will undergo efficient and reversible anionic redox. The present finding provides insights into new directions to be explored for the development of high-energy density materials for Li-ion batteries.

1

I. INTRODUCTION

The Li-ion technology has been the subject of intensive research since the first observation of reversible Li intercalation in Li_xTiS_2 by Exxon in 1976.[1] However safety issues associated with the dendritic growth of Li at the electrode surface discarded the Li-based technology as suitable for commercialisation. Attempts to circumvent this lock have led to the emergence of the Li-ion concept in the 80s and the first commercialisation of the $LiCoO_2/C$ Li-ion technology by Sony in 1991. The current state-of-the-art positive electrodes use either the layered $LiCoO_2$ [2,3] structure or its tri-dimensional derivatives $LiMn_2O_4$[4] or combined compositions,[5] or polyanionic compounds among which $LiFePO_4$[6] is poised to play a major role in the near future. Todays research is parted between two schools: one favouring safety and cost to the expense of energy density lowered by the use of heavy inactive polyanions, and the other giving more importance to energy density hence continuously optimizing the $LiCoO_2$ chemistry. Even though both have led to rich discoveries, this paper focuses on the latter.

The use of transition metal (TM) oxides as positive electrode materials in Li-ion batteries was first proposed by Goodenough in the early 80s,[2] but was further limited by severe drawbacks.[7,8] Only 50% of the theoretical capacity of the layered $LiCoO_2$ electrode can be exploited in Li-ion cells (145 mAh/g instead of 270 mAh/g) to avoid material degradation.[3] To limit this issue, chemical substitutions of the Co^{3+} ions were proposed to stabilize the layered structures by minimizing the electrostatic repulsions between consecutive MO_2 layers in the delithiated members. This has led in the early 2000s to the discovery of the $Li(Ni_{1/3}Mn_{1/3}Co_{1/3})O_2$ layered oxides coined as NMC,[9–11] which display much higher capacities (180 mAh/g) than the three-dimensional spinels, e.g. $LiMn_2O_4$[4] and $LiNi_{0.5}Mn_{1.5}O_4$ ($\sim$ 140 mAh/g)[12] or the most performing polyanionic compound $LiFePO_4$ (170 mAh/g).[6] These Li-NMC electrodes are progressively replacing $LiCoO_2$ in todays Li-ion cells. Further explorations of cationic substitutions in the layered oxide systems[13] back to 2006 led to materials made of Ni, Co and Mn with some Li in the metallic layers, in addition to the Li present in the Van der Waals gap, hence leading to materials known as Li-rich NMC showing capacities exceeding 280 mAh/g. Despite their impressive capacities, the commercialization of the Li-rich NMC is still compromised due to potential fade[14] and irreversible O_2 gas

release upon charge.

Recently, new chemistry was explored with the Li_2MO_3 family of compounds having the same layered structure and more Li within the metal layers than the Li-rich NMC, but deviating from the classical route by using $4d$ rather than $3d$ metals. Among these materials, the model $Li_2Ru_{1-y}Sn_yO_3$ phases exhibit similar capacities of 260 mAh/g as Li-rich NMC but neither capacity fading nor O_2 gas release upon cycling.[15] The origin of the large capacity was attributed to a cumulative cationic and anionic redox activity.[15] The anionic contribution was then proposed to be associated with a reversible oxo- (O^{2-}) to peroxo-like $(O_2)^{n-}$ transformation upon charge/discharge and driven by a reductive coupling mechanism.[15] This mechanism was further demonstrated through Electron Paramagnetic Resonance (EPR) measurements in $Li_{2-x}Ru_{0.75}Sn_{0.25}O_3$[16] and more recently through high-resolution microscopy in $Li_{2-x}IrO_3$[17] which exhibits an O_1-type stacking of the metallic layers allowing clear visualization of the O-O dimers. However, the formation of peroxo-like species often results in O_2 gas release for some systems with no clear rationalization of the role of the transition metal on this phenomenon.[18,19]

The promotion of a reversible anionic redox in TM-based materials is recognized as being triggered by the degree of metal-ligand (cation-anion) covalent bonding since the early work of Rouxel on layered TM-dichalcogenides[20,21] and was further discussed as ligand hole chemistry in transition metal oxides by Tarascon in 1999.[22] From a fundamental point of view, the degree of metal-ligand covalency is a property of the material ground state and arises from the interplay between the d-d Coulomb repulsions (namely U) and the metal-ligand electronegativity difference known as the charge transfer (namely Δ).[23] Ever since, TM-based materials with an enhanced degree of covalency compared to TiX_2 (X = S, Se, Te) were developed to exploit the anionic redox as a lever to increase materials specific capacity. As an example, TM-phosphides[24,25] of the Li_xMP_4 (M = $3d$ metal; x = 1 to 11) family can exchange up to 10Li per transition metal with no significant structural change upon lithiation/delithiation leading to specific capacities as high as 1000 mAh/g. In perfect agreement with the Goodenough rule on the ligand inductive effect,[26] these materials exhibit low working voltages around 1.5 V which prevents their use as cathode materials in Li-ion batteries. Focusing on the energy density, the necessary condition is to increase the

capacity while maintaining a high redox potential. This inevitably appeals to compromise since one is generally detrimental to the other.[27] In TM-oxides, one strategy was directed to the substitution of M($3d$) for M($4d$) and even M($5d$) with the hope that their lower chemical potentials and greater ability to make strong covalent M-O bonds could efficiently balance the subsequent increase of molar weight by involving the oxygen redox couples.

So far, numerous computational studies have been devoted to the electrochemical properties of various layered TM-oxides. Most of these studies deals with the impact of (i) Li/M ordering,[28] (ii) cationic migration paths,[29,30] (iii) phase transitions[31] and (iv) material thermal stability[32] on the electrochemical performances of the materials but, to our knowledge, there is no study dedicated to the oxygen network response upon delithiation. Addressing the intriguing role of the anions in the electronic and structural response of layered TM-oxides and the origin of the O_2 release is then required to determine whether or not a winning combination of cations and anions exists that could make these systems suitable for applications. The present paper aims at identifying robust descriptors to rationalize the anionic redox mechanism in the layered Li-rich TM-oxides using conceptual tools, such as atomic charges, orbital interactions and crystal orbital overlap populations (COOP) all based on first-principles Density Functional Theory (DFT) calculations.

II. RESULTS

The Li_2MO_3 family of compounds is an extension of the $LiMO_2$ and Li-rich $Li_{1+x}M_{1-x}O_2$ series through the increase of the Li^M/M ratio in the metallic layers. These phases are all described in the same general formulation $Li[Li_x^M M_{1-x}]O_2$ where x is set by the transition metal oxidation state n through the relation $x = (n-3)/(n-1)$. The progressive increase of the Li^M/M ratio from $LiM^{3+}O_2$ to $Li_2M^{4+}O_3$ then results in a progressive increase of the average transition metal oxidation states in the layers to compensate the lack of cationic charges. Because the Li_2MO_3 series displays various electrochemical activity vs. Li from a classical cationic redox to either a reversible anionic redox or an irreversible O_2 release,[15,18,19,33–37] they are relevant model structures to investigate the role of M($4d$) vs. M($3d$) on their electrochemical behavior. Here we use different model calculations within the framework of Density Functional Theory (DFT) to discriminate the electronic, ionic

4

and structural responses of the systems to the electrochemical oxidation and to get more insights in the microscopic mechanisms related to oxygen redox activity in the Li-rich layered TM-oxides.

A.   The case of $4d$-metals

As a test case for the M($4d$), we investigated the $Li_{2-x}RuO_3$ phases from first-principles DFT calculations. As shown in Fig. 1, the Density Of States (DOS) of Li_2RuO_3 confirms that the oxygen contribution to the bands lying around the Fermi level is significant, although in minority compared to the transition metal contribution. This agrees with the strongly covalent Ru-O bonds in this system[23] which are therefore expected to be the *redox active center* of the electrochemical reaction.[27] Assuming a rigid band picture, the removal of two consecutive electrons from the Li_2RuO_3 electronic structure leads to a shift of the Fermi level down to ε_F^1 and ε_F^2 (see Fig.1) and reveals that the band involved in the oxidation process has a mixed Ru/O character with still a dominant metallic contribution. This suggests a dominant cationic redox activity for the $Li_{2-x}Ru^{4+x}O_3$ electrode with some delocalization of the created holes over the Ru-O bonds.

When lithium is also removed (i.e. $-Li^+ -e^-$) from the Li_2RuO_3 structure without allowing structural relaxation, the story is different. The band lying just below the Fermi level of $LiRuO_3$ now exhibits a predominant oxygen character (Fig. 1b) showing that the O-band is raised in energy when Li is removed. The structure being here unchanged, this destabilization can solely be attributed to the loss of compensating Li^+ positive charges in the first neighboring shell of the O^{2-} anions which lowers the electrostatic Li-O energy. The charge density differences computed for the two successive oxidation processes (namely $\Delta\rho^{Li_2 \to Li_1}$ and $\Delta\rho^{Li_1 \to Li_0}$ in Figs. 1f-i) give a direct visualization of the regions in space where the hole (yellow volume) is localized when removing either two consecutive electrons (rigid band approach, RB) or two consecutive lithium (rigid structure approach, RS) from Li_2RuO_3. What makes the comparison between the two approaches valuable is that it allows discriminating the electronic and ionic contributions to the system redox activity. For the first oxidation process, a cationic redox is equivalently predicted by the two approaches:
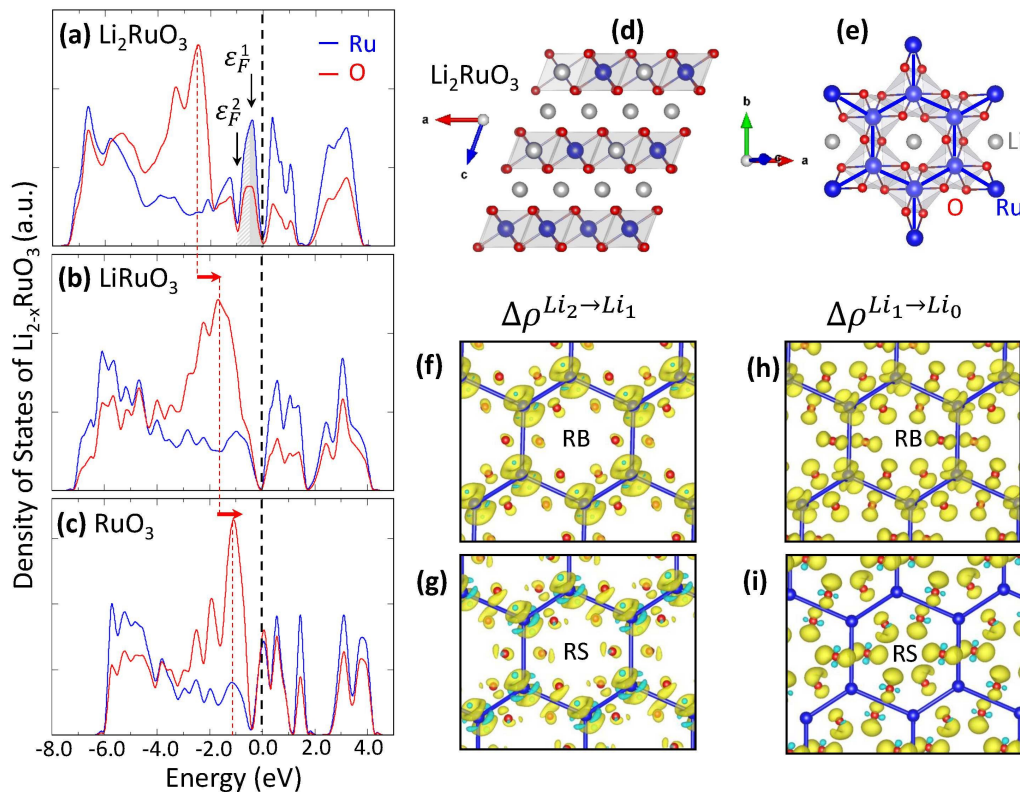
5

FIG. 1. **Rigid band vs. rigid structure approaches to the oxidation processes:** (a-c) Density of states (DOS) of the $Li_{2-x}RuO_3$ ($x = 0, 1, 2$) computed within the DFT+U framework using the crystal structure of the fully lithiated phase ($x = 0$) represented in the right top panel along the **c**-axis (d) and within the layer planes (e). The Fermi level is set at the zero energy and is illustrated by the vertical dotted black line. The Fermi level corresponding to the removal of 1 (ε_F^1) and 2 (ε_F^2) electrons from a rigid band approach are indicated on (a). The O-band destabilization induced by the removal of two consecutive Li is indicated by the red arrow on (b) and (c). Charge density differences between Li_2RuO_3 and $LiRuO_3$ ($\Delta\rho^{Li_2 \to Li_1}$) and between $LiRuO_3$ and RuO_3 ($\Delta\rho^{Li_1 \to Li_0}$) computed within the rigid band model RB (f,h) and rigid structure model RS (g,i) and plotted in the metallic plane where Ru and O are represented by blue and red spheres, respectively. Li atoms are omitted for a sake of clarity. The yellow volumes correspond to electron density depletion (holes) while the small cyan regions correspond to electron density accumulation (electrons) due to orbital polarisation.

both $\Delta\rho^{Li_2 \to Li_1}$ computed in RB (f) and RS (g) show that the holes (yellow volumes) are mostly localized on the transition metal ions (blue spheres) with however a slightly larger contribution on the oxygen (red spheres) in the RS model. Note that the small cyan regions displayed on the $\Delta\rho^{Li_2 \to Li_1}$ RS correspond to electron density accumulation and indicate that the metallic d-orbitals are weakly polarized through $4d \to 4d$ charge transfer when Li is removed. In contrast, the second oxidation process is strongly influenced by the Li^+ removal: while the RB model predicts a mixed cationic/anionic activity with holes almost equivalently spread over Ru and O (h), the RS model shows a purely anionic activity with holes exclusively localized on O (i). This anionic activity corresponds to the formation of unstable $O^{(2-1/3)-}$ species due to the O-band destabilization mentioned above and demonstrates the dynamical response of the material electronic structure to the variation in lithium composition, through the modification of its electrostatic potential.

How the system structurally responds to the creation of these unstable electron holes on the oxygens (hereafter denoted O-holes) was then investigated through the relaxation of the $Li_{2-x}RuO_3$ structures at each Li-composition ($x = 0, 1, 2$). As shown in Fig. 2 (top panel), the oxygen network is not significantly affected during the first oxidation process from Li_2RuO_3 to $LiRuO_3$ in agreement with the main cationic redox expected from the two previous approaches. The DOS of the relaxed $LiRuO_3$ shows that the O-band is only slightly shifted down to lower energies compared to the RS approach (see Supplementary Figure SI1) which indicates that both the RB or RS approaches give a correct picture of the redox process, as for all high-potential cathode materials in which the Li-reactivity is governed by the transition metal as the main redox active centre.[27] For the second oxidation process from $LiRuO_3$ to RuO_3, the oxygen network is now strongly modified: three of the six O-O distances of the RuO_6 octahedra decrease from ca. 2.80 Å in the partially lithiated $LiRuO_3$ material to ca. 2.32 Å in the fully delithiated RuO_3 material, while the Ru-O distances are only slightly shortened from 1.96 to 1.91 Å. The O-band lying below the Fermi level is also significantly lowered in energy compared to the RS model (see Supplementary Figure SI1) showing that the distortion of the O-network is stabilizing for the system. The scenario of oxo- to peroxo-like transformation $(2O^{2-}/(O_2)^{n-})$ recently reported for other Ru-based $Li_2Ru_yM_{1-y}O_3$ electrodes[15,18,19] (M = Ti, Mn, Sn) is then observed in the pure Ru-based compound, as well, showing that it is not linked to the ancillary metal.
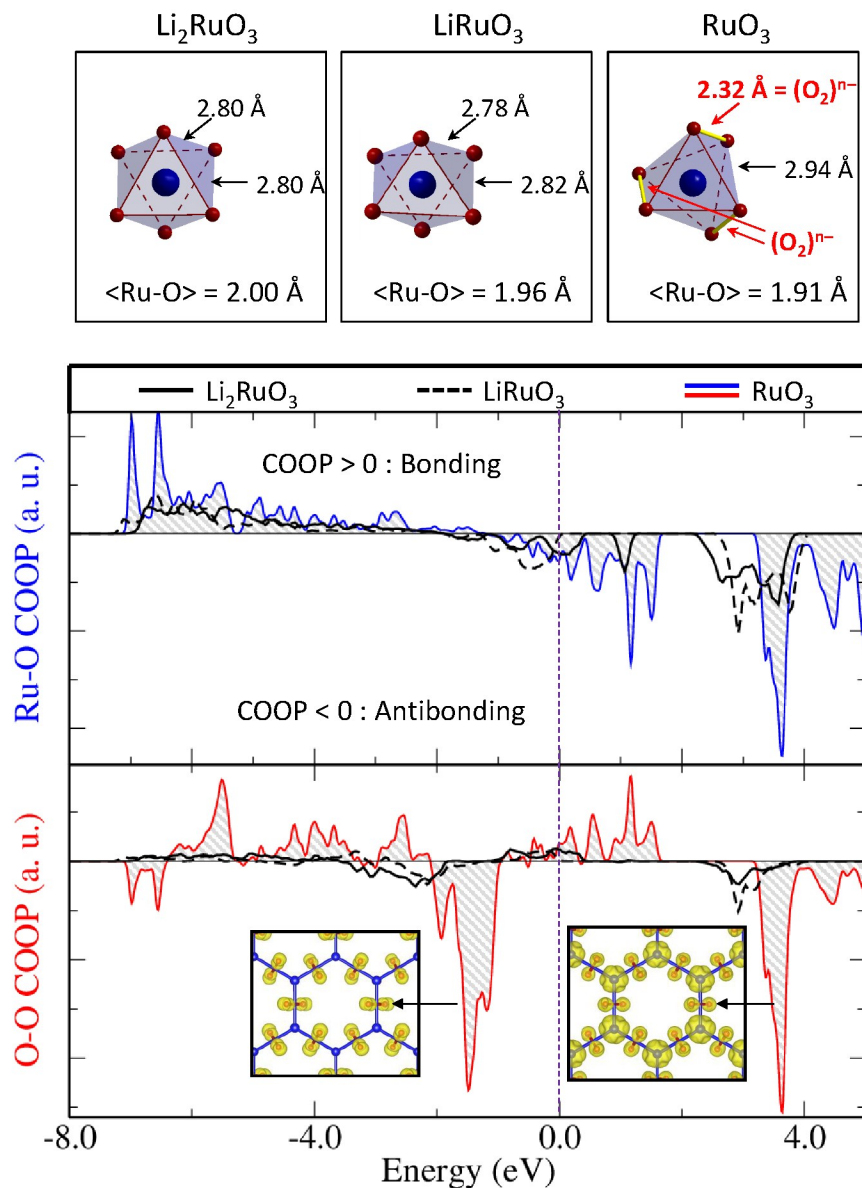
FIG. 2. **Direct visualization of oxo to peroxo $2O^{2-}/(O_2)^{n-}$ transformation upon delithiation:** Local environment of the Ru cations (O-O distances and average <Ru-O> distances) and COOPs computed from DFT+U calculations for the Ru-O bonds (between 1.8 and 2.2 Å) and O-O bonds (between 2.2 and 2.4 Å) in the relaxed $Li_{2-x}RuO_3$ structures at $x = 0$ (black), 1 (dotted black) and 2 (blue and red for Ru-O and O-O, respectively). The formation of the O-O bonds is clearly visualized by the increase in the O-O COOPs amplitude during the $LiRuO_3$ to RuO_3 oxidation process. The electron density maps computed for the bands exhibiting the most antibonding O-O character (inset of O-O COOPs) confirm the polarization of the O(2p)-orbitals towards the O-O axis required to form σ-type O-O bonds.

To identify the formation of O-O bonds in the $Li_{2-x}RuO_3$ structures, we plot their Crystal Orbital Overlap Populations (COOPs) at each composition. This tool is a powerful bonding descriptor which is constructed by generating an overlap population-weighted density of states. In addition to the projected DOS which give the relative participation of each atomic levels in the electronic band structure of the system, the COOPs add the overlap dimension by showing the bonding (COOP > 0), non-bonding (COOP $= 0$) or antibonding (COOP < 0) character of each electronic state over the system chemical bonds.[38,39] They have been computed for the Ru-O and O-O bonds in the relaxed $Li_{2-x}RuO_3$ phases for $x = 0$, 1 and 2 and are plotted in Fig. 2. As expected in TM-oxides,[23,27] the Ru-O COOPs are mostly bonding (> 0) below the Fermi level (MO-band) and mostly antibonding (< 0) around the Fermi level (MO*-band) while pure oxygen levels lie in between (O-band). Following the small Ru-O bond shortening upon delithiation (increase of the $Ru(4d)/O(2p)$ overlap), the bonding Ru-O levels are pushed down to lower energies from Li_2RuO_3 (solid black line) to $LiRuO_3$ (dotted black line) and RuO_3 (blue curve), so as the antibonding Ru-O levels are pushed up to higher energies.

Regarding the O-O COOPs, they are negligible for Li_2RuO_3 (solid black line) and $LiRuO_3$ (dotted black line) in agreement with the long O-O distances (ca. 2.8 Å) occurring in these two phase compositions which prevent significant $O(2p)/O(2p)$ overlap and therefore O-O chemical bonds. The O-O COOPs become significant during the second oxidation process with the appearance of intense bonding and antibonding peaks for RuO_3 (red curve). The electron density maps computed for the two intense antibonding peaks around the Fermi level at ca. -1.8eV and +3.8eV show that the $O(2p)$-orbitals are polarized towards the O-O bond axis through a σ-type overlap. These pieces of information clearly indicate the formation of σ-type O-O bonds in the RuO_3 compound, as a direct consequence of electron removal from strongly antibonding O-O σ^* electronic levels. The fact that one-third of the σ^* antibonding states are emptied for RuO_3 indicates an O-O bond order lower than one (see Supplementary Figure SI2), in full agreement with the rather long O-O distances observed in RuO_3 (2.3 Å) compared to known peroxides (1.5 Å) and with the $n \geq 3$ charge of the $(O_2)^{n-}$ species proposed for the Ru-based materials from EPR analysis.[16]
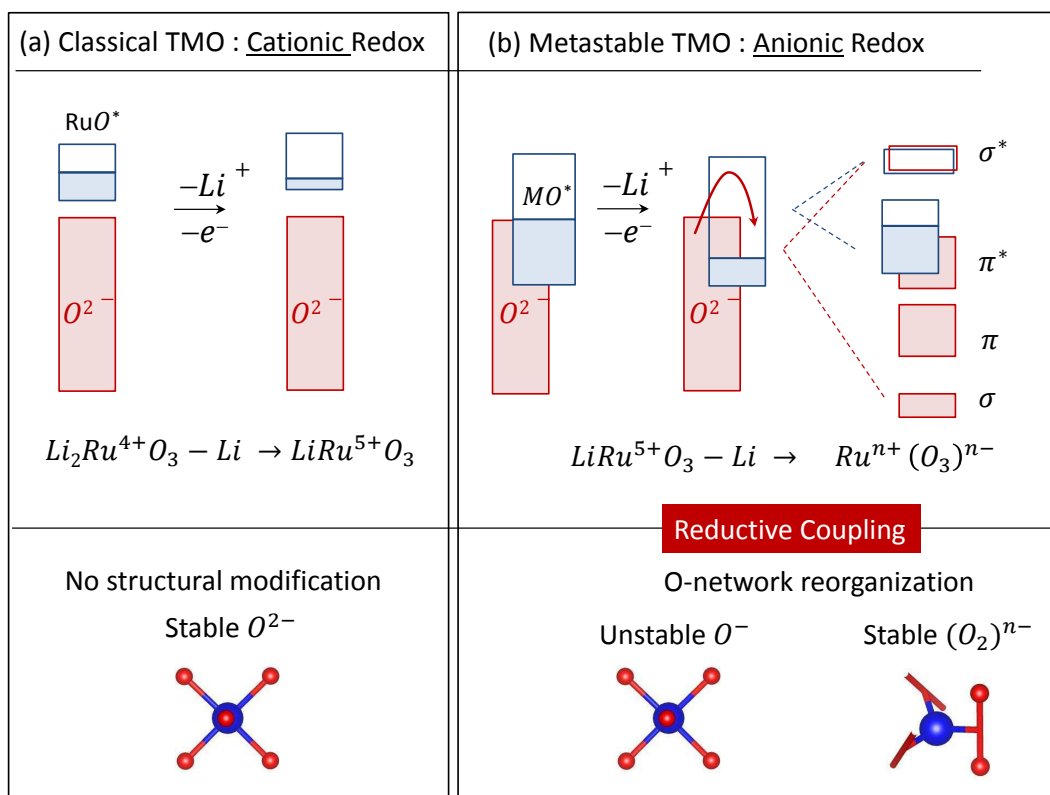
FIG. 3. **Cationic vs. Anionic redox:** Qualitative band structure of a structurally stable (a) and metastable (b) transition metal oxide described by strongly covalent M-O bonds and therefore almost equivalent contributions of M and O to the redox band. After a classical cationic redox associated with the removal of 1Li, further Li-extraction induces an unstable transition state which is dynamically stabilized through a $2O^{2-} \rightarrow (O_2)^{2-}$ transformation catalyzed by the transition metal. The mechanism uses the M-O bond covalency to split the O($2p$)-band in order to stabilize the O-holes. It is associated with a significant modification of the transition metal environment illustrated by local MO_6 entities. In the case where a complete $2O^{2-}/(O_2)^{2-}$ transformation occurs, the transition metal is inevitably reduced since the removal of 1Li does not allow compensating the system charge.

This theoretical investigation of the $Li_{2-x}RuO_3$ confirms the cumulative cationic and anionic redox activity previously reported for other Ru-based $Li_{2-x}Ru_yM_{1-y}O_3$ (M = Sn, Mn, Ti) systems,[15,18,19] and allows rationalizing the mechanism of the oxo- to peroxo-like transformation $(2O^{2-}/(O_2)^{n-})$. As shown schematically in Fig. 3, $Li_2Ru^{4+}O_3$ first undergoes a classical cationic oxidation to form the (structurally close) $LiRu^{5+}O_3$ phase. Then the $LiRu^{5+}O_3$ phase undergoes an anionic oxidation that creates unstable O-holes on the

oxygen network, therefore triggering its reorganisation. The $2O^{2-}/(O_2)^{n-}$ transformation is catalyzed by the transition metal which allows for Ru($4d$)-$O_2(\sigma)$ covalent interactions, therefore stabilizing the O-holes through their delocalization over Ru-O and O-O σ-type bonds. This mechanism is called a reductive coupling mechanism as the formation of O-O dimers induces a O $\longrightarrow$ M charge transfer illustrated by atomic charge Bader analysis (see Supplementary Table SI1). Therefore, as long as the peroxo-like $(O_2)^{n-}$ species are covalently bonded to the transition metal through M(d)-$O_2(\sigma)$ interactions, the anionic redox should be reversible, thus increasing the material capacity.

B. The case of $3d$-metals

For a sake of comparison, we investigated the $Li_{2-x}MnO_3$ phases, following the same procedure as the one described above for $Li_{2-x}RuO_3$. Experimentally, this electrode shows a limited redox activity[34–37,40,41] compared to its Ru-based analogue,[15] with evidence of significant O_2 release and layered to spinel-like phase transition upon delithiation. Its layered structure, similar to that of Li_2RuO_3, makes Li_2MnO_3 a perfect model to investigate the impact of M($4d$) by M($3d$) chemical substitution on the electrochemical behavior of Li-rich layered TM-oxides. Compared to $Li_{2-x}RuO_3$, $Li_{2-x}MnO_3$ exhibits different electronic and structural responses upon Li removal. First, its electronic structure shows a predominant contribution of oxygen electronic states at the Fermi level, indicative of a pure anionic activity from the very first Li-removal (see Supplementary Figure SI3). As displayed on the schematic picture of Fig. 4, the structural response of the system to the creation of O-holes leads to a condensed layered MnO_3 phase characterized by a strongly reduced interlayer spacing arising from the formation of very short interlayer O-O bonds around 1.40-1.50 Å. Concomitantly to the O-O bond shortening, a significant Mn-O bond elongation is observed from 1.90 Å in $LiMnO_3$ to 2.15 Å in MnO_3 which suggests a partial decoordination of the O-O dimers from the metallic network. The analysis of the Mn-O and O-O COOPs given in Supplementary Figure SI3 confirms this decoordination by showing that the O-O dimers are no longer bonded to Mn (negligible Mn-O COOPs) and strongly oxidized to $(O_2)^{n-}$ with $n \leq 2$ (at least the (O_2)-σ^* antibonding levels are emptied). The reductive coupling mechanism observed in $Li_{2-x}RuO_3$ to stabilize the $(O_2)^{n-}$ peroxo-like species in the structure through covalent Ru-(O_2) bonding does not occurs in $Li_{2-x}MnO_3$ due to the lack of Mn-O

covalency. Instead, a reductive elimination is predicted for MnO_3 leading to a significant reduction of the transition metal to compensate for the formation of strongly oxidized O-O dimers (see Supplementary Table S1).
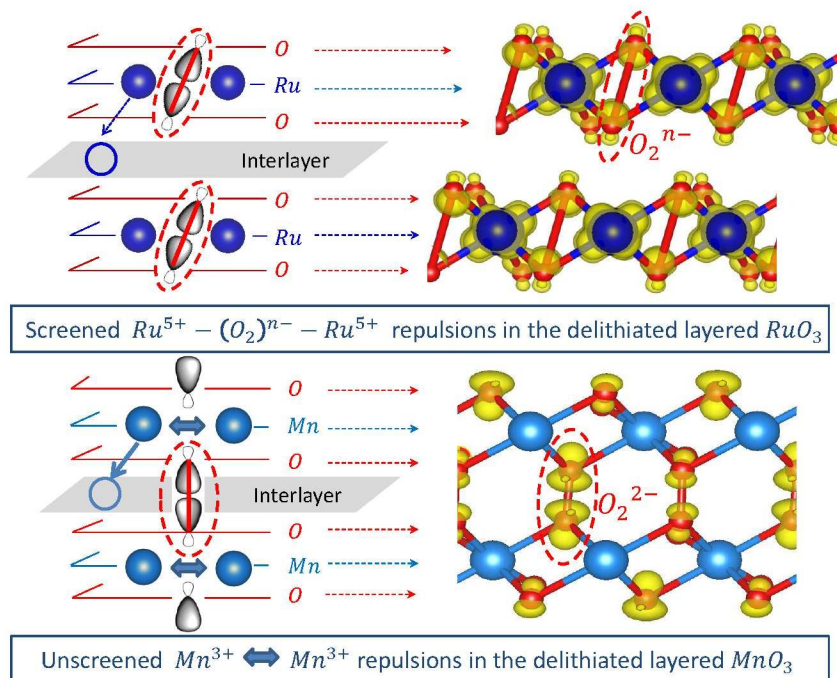

FIG. 4. **Differences in the electronic and structural responses of the $Li_{2-x}RuO_3$ (top) and $Li_{2-x}MnO_3$ (bottom) phases from $x = 1$ to 2:** The formation of short O-O bonds in the RuO_3 and MnO_3 phases induces a polarization of the O_2 electron density through the σ-type bonding towards the metallic layer for Ru and towards the lithium layer for Mn. The consequence of this polarisation on the cation-cation electrostatic repulsions in the metallic layer is highlighted as a trigger to Mn migrations.

These results are compatible with the oxygen evolution experimentally observed for this phase upon delithation,[40,41] although no experimental evidence for metallic reduction has been reported. Noteworthy that if O_2 release is massive and preferentially occurs at surfaces, a partial surface decomposition of MnO_3 to MnO_2 could explain why Mn^{3+} is not observed. In fact, the delithiated layered MnO_3 phase is known to be metastable and prone to Mn migrations from the metallic layer to the lithium layer via tetrahedral site to form a "spinel-like" phase.[30,37,42] Using first-principles DFT calculations, Lee and Persson[42,43] have recently shown that the cationic migration in $Li_{2-x}MnO_3$ is thermodynamically favored at $x \geq 1$ and kinetically activated by a cooperative complex mechanism involving the oxygen network at

very low-lithium content ($x \sim 0$). Mohanty et al.[37] used neutron powder diffraction to show that the migration of Mn from octahedral to tetrahedral sites should start at V > 4.1 Volt. Three of our observations are at least in line with these results: (i) the formation of short O-O interlayer bonds which induces a depletion of anionic charges in the metallic layers, therefore increasing the cation-cation electrostatic repulsions; (ii) the partial decoordination of the O-O dimers from the metallic network which frees the Mn migration and (iii) the Jahn-Teller instability of octahedral Mn^{3+} ions which is favorable to Oh $\longrightarrow$ Td migration. It is thus likely that a concerted mechanism takes place in this system to stabilize both the O-holes (formation of short O-O interlayer bonds) and the MnO_3 crystal structure (Mn migrations). The former should be kinetically and thermodynamically favored above a critical Li-composition $1 < x \leq x_c$ for which the Li-content in the interlayer is low enough to allow O-O bond shortening but too high to activate the Oh$\longrightarrow$Td channels for Mn migration. The latter should become dominant at $x > x_c$ where the Li-layers are almost vacant, therefore opening low energy paths for Mn migration. The fact that Mn migration limits the O-O bond shortening is consistent with the longer interlayer spacing found by Lee and Persson[42] in the "spinel-like" MnO_3 (2.36 Å) compared to the layered MnO_3 (1.50 Å) as well as with a lower Mn reduction than the one given by our Bader charge analysis (see Supplementary Table SI1). The onset of this concerted mechanism should naturally be hindered at surfaces, thus triggering the O_2 evolution reported for this system upon charge.[34–37,40,41]

III. DISCUSSION

The present study allows clarifying the different ways oxygen contributes to the redox activity of Li-rich layered TM-oxides. As depicted in Fig. 5, the cationic redox activity arises in classical TM-oxides when the Fermi level lies in the band arising from M-O antibonding electronic levels (MO*-band). In this scenario, the contribution of the oxygen to the redox band is lower than that of the transition metal although the anions do participate in the redox activity of the system through the lowering of the electrochemical potential.[26,27] This case of cationic redox is exemplified by the $Li_2Ru^{4+}O_3$ -Li $\longrightarrow$ $LiRu^{5+}O_3$ oxidation process.

The anionic redox is activated as soon as the bottom portion of the O-band merges the

Fermi level. The process is reversible if and only if the metastable O-holes created upon oxidation can be stabilized through the formation of $(O_2)^{n-}$ peroxo-like species that remain covalently bonded to the transition metal. This can be achieved through a TM-driven reductive coupling mechanism that prevents O_2 gas release or drastic structural reorganization leading to phase transition. This case of reversible anionic redox is exemplified by the $LiRu^{5+}O_3$ -Li $\longrightarrow$ $LiRu^{5+}[(O_2)^{3.333-}]_{3/2}$ oxidation process.

What makes the reductive coupling mechanism interesting is that, in principle, it could allow the transition metal to be formally reduced upon oxidation thus providing routes for improving the capacity of high-potential materials. Indeed, if we assume a complete $2O^{2-}/(O_2)^{2-}$ oxo-peroxo transformation when removing 2Li from the $Li_2M^{4+}(O^{2-})_3$ structure, the charge equilibration would lead to $M^{3+}[(O_2)^{2-}]_{3/2}$ as resulting from an internal redox process between the MO*-band and the O-band here acting as a reservoir of electrons (in charge) and holes (in discharge). If more lithium per transition metal were available in the structure, this could open the way to further delithiation as already observed in the Li_xMP_4 compounds for which 10Li/TM can be reversibly exchanged during charge/discharge.[24,25]

Eventually the oxygen may participate to the electrochemical activity of the system through an irreversible oxidation process which ultimately ends with O_2 gas release. This scenario corresponds to an electronic instability of the TM-oxides and leads to a partial or complete decoordination of the $(O_2)^{n-}$ species due to a lack of M-O covalency. This scenario is exemplified by the $Li_{2-x}MnO_3$ electrode and occurs when the O-band overlaps the MO*-band in such a way that there is no empty MO*-orbitals close enough to the top portion of the O-band to trigger the reductive coupling mechanism. This situation may appear when the MO*-band is either too narrow (no itinerant electrons) or when it exhibits a large Mott band gap (strongly correlated half-filled $3d$ metals).[23,44] In that case, the DOS of the material at the Fermi level exhibits a dominant oxygen character and the oxidation process creates unstable O-holes on the O-network with no route to stabilize the created O_2^{n-} species through M-(O_2) covalent interactions. The formation of such decoordinated $(O_2)^{n-}$ species is expected to occur at potentials lower than 4.3 Volt then leading to a (O_2) gas release above this value.

The present study then rationalizes the electrochemical properties of the Li-rich Li_2MO_3
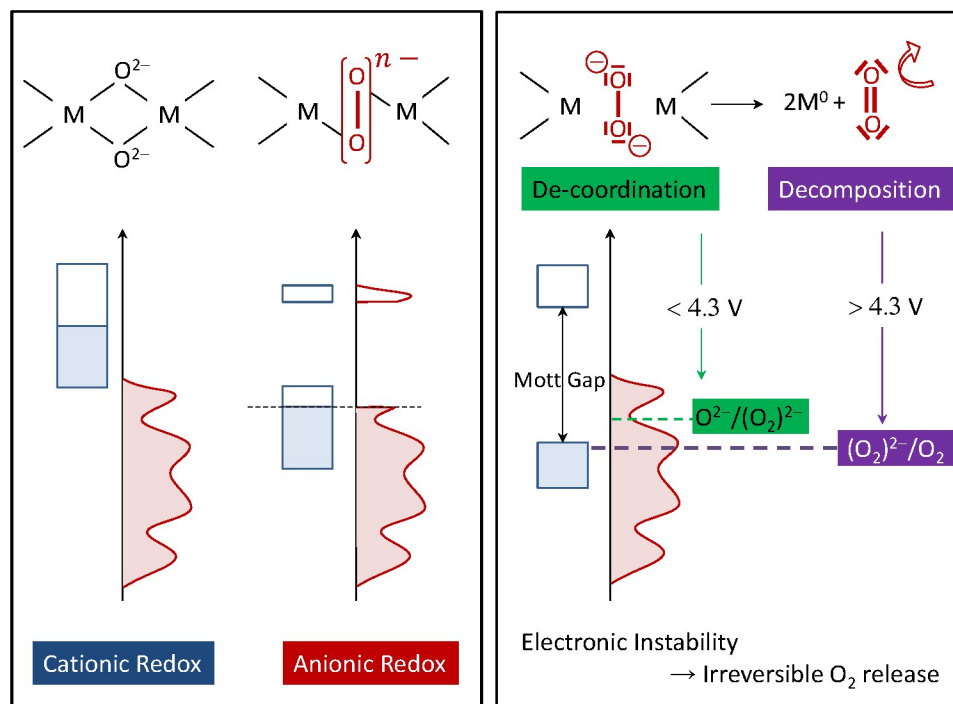
FIG. 5. **Oxygen Participation to the Redox Activity of a TM-oxides:** Schematic representation of the three different redox activity of a transition metal oxide along with the associated Lewis structures of the oxygen species. The oxo O^{2-} and peroxo-like $(O_2)^{n-}$ species occur during a reversible cationic and anionic redox, respectively while the peroxo $(O_2)^{2-}$ species start to de-coordinate the transition metal prior to be fully oxidized in O_2 gas through a complete reductive elimination. The green and purple horizontal lines refer to the redox energies of the $2O^{2-}/(O_2)^{2-}$ and $(O_2)^{2-}/O_2$ transformation, respectively

family of compounds in terms of three possible mechanisms: a reversible cationic redox, a reversible anionic redox and an irreversible O_2 gas release. The use of model calculations to discriminate the electronic, ionic and structural responses of Li-rich TM-oxides to Li removal is here shown to be very powerful to figure out the microscopic mechanisms at the origin of these various electrochemical behaviors. Of significance to the battery community, the oxygen contribution immediately below the Fermi level is not the proper descriptor to predict the extent of M-O covalency, though it is often used as such. We here propose to use combined DOS and COOP analyses as a means to determine the cationic vs. anionic and reversible vs. irreversible redox activity taking place in a given system. These combined

tools enable us to evaluate the O-band participation in the system redox activity but more importantly to understand how strongly it interacts with the metal orbitals to stabilize the $(O_2)^{n-}$ peroxo-like species through a reductive coupling mechanism. The M-(O_2) covalent bonding is here shown to be an absolute condition for the anionic redox to be reversible. In the case of M($4d$), the extra-capacity arising from the oxygen network is limited to 1 electron (formation of $(O_2)^{3.33-}$ peroxo-like species) probably due to symmetry constraints. The M($4d$) vs. M($3d$) comparaison clearly higlights that the M($3d$)/O($2p$) overlap is not sufficient for a reductive coupling mechanism to take place. The occurrence of pure oxygen electronic levels at the Fermi level in the electronic structure of Li_2MnO_3 is a clear indicator of the metastability of this phase with respect to O_2 release, which should preferentially occurs at surfaces. The lack of Mn($3d$)-O($2p$) covalent bonding is responsible for the decoordination of the $(O_2)^{n-}$ species from the metallic network, therefore triggering the Mn migration at the origin of the layered to spinel transition. It is therefore not surprising that mixing $4d$- and $3d$- metals lead to better material stability vs. O_2, as recently experienced by Yabuuchi et al.[33] Nevertheless, since the capacities in these materials are already extremely high, it is now critical to limit the cationic migrations. This might be achieved by increasing the Li^M/M ratio in the metallic layer to form Li-extra-rich $Li_{2+x}M_{1-y}O_3$ (e.g. Li_3MO_4) as recently exemplified with Nb-based electrodes.[33] This would allow retaining Li (or heavier alkali, namely Na, K) in the Li-layer to limit the driving force of M migration. Heavier or larger size metals should also limit M migration as recently demonstrated in the Li_2IrO_3 layered material but might be too penalizing for the material weight and cost.[17] Another approach might use controlled oxygen to sulfur chemical substitutions to increase the M($3d$)/O-S(np) overlap and hopefully activate the reductive coupling mechanism with $3d$-metals without affecting too much the material potential. We hope that the knowledge gained from this study through the use of pertinent descriptors aiming at identifying which type of redox should dominate the electrochemical activity of a given material, will guide the selection of optimized cationic-anionic redox pairs in order to promote anionic redox processes while limiting the $(O_2)^{n-}$/O_2 recombination process leading to oxygen release. Ultimately, we hope this work will stimulate further work for designing advanced high energy density electrode materials and benefit other energy-related fields relying on ligand-hole chemistry such as electrocatalysis and superconductivity.

IV. METHODS

Spin-polarized density functional theory (DFT) calculations were performed using the plane-wave density functional theory (DFT) VASP code (Vienna Ab initio Simulation Package).[45,46] within the generalized gradient approximation of Perdew-Burke-Ernzerhof (PBE) to describe electron exchange and correlation.[47] The rotationally invariant Dudarev method[48] (DFT+U) was used to correct the self-interaction error of conventional DFT for correlated d-electrons. Different U parameters varying from 0 to 4 eV for Ru and 4 to 5 eV for Mn were tested which led to slightly different crystal structures, DOS and COOP but did not affect the trend of the redox mechanism presented in this paper. Spin-orbit coupling was introduced with no significant change on the redox properties of the $Li_{2-x}RuO_3$ systems. Pristine structures before relaxation for Li_2RuO_3 and Li_2MnO_3 were taken from the literature[49,50] and several Li-distributions were considered for Li-removal. For a sake of comparison we have restrict our studies to the perfectly ordered Li_2MO_3 phases where Ru and Mn lie at the corner of the honeycomb layer. All atom coordinates and lattice parameters were fully relaxed using conjugate gradient energy minimization untilthe forces acting on each atom were less than 5.10^3 eV/ $Å^2$.A plane-wave cutoff of 600 eV was used to define the basis set, with well-converged k-point sampling for each compound. The COOP were computed using the Lobster program developed by Dronskowski and coworkers.[39,51,52]

---

[1] M. Whittingham, *Progress in Solid State Chemistry*, 1978, **12**, 41–99.

[2] K. Mizushima, P. C. Jones, P. J. Wiseman and J. B. Goodenough, *Materials Research Bulletin*, 1980, **15**, 783–789.

[3] J. N. Reimers and J. R. Dahn, *Journal of The Electrochemical Society*, 1992, **139**, 2091–2097.

[4] M. Thackeray, W. David, P. Bruce and J. Goodenough, *Materials Research Bulletin*, 1983, **18**, 461–472.

[5] M. M. Thackeray, C. S. Johnson, J. T. Vaughey, N. LiCurrent address: eVionyx Inc., Ha and S. A. Hackney, *Journal of Materials Chemistry*, 2005, **15**, 2257–2267.

[6] A. K. Padhi, K. S. Nanjundaswamy and J. B. d. Goodenough, *Journal of the Electrochemical Society*, 1997, **144**, 1188–1194.

[7] J. Dahn and W. McKinnon, *Solid State Ionics*, 1987, **23**, 1–7.

8 C. Delmas, C. Fouassier and P. Hagenmuller, *Physica B+C*, 1980, **99**, 81–85.

9 T. Ohzuku and Y. Makimura, *Chemistry Letters*, 2001, 642–643.

10 Z. Lu, D. D. MacNeil and J. R. Dahn, *Electrochemical and Solid-State Letters*, 2001, **4**, A200.

11 C. Johnson, J.-S. Kim, C. Lefief, N. Li, J. Vaughey and M. Thackeray, *Electrochemistry Communications*, 2004, **6**, 1085–1091.

12 J.-H. Kim, S.-T. Myung, C. S. Yoon, S. G. Kang and Y.-K. Sun, *Chemistry of Materials*, 2004, **16**, 906–914.

13 Z. Lu, L. Y. Beaulieu, R. A. Donaberger, C. L. Thomas and J. R. Dahn, *Journal of The Electrochemical Society*, 2002, **149**, A778.

14 X. Zhang, X. Meng, J. W. Elam and I. Belharouak, *Solid State Ionics*, 2014, **268**, 231–235.

15 M. Sathiya, G. Rousse, K. Ramesha, C. P. Laisa, H. Vezin, M. T. Sougrati, M.-L. Doublet, D. Foix, D. Gonbeau, W. Walker, A. S. Prakash, M. Ben Hassine, L. Dupont and J.-M. Tarascon, *Nature Materials*, 2013, **12**, 827–835.

16 M. Sathiya, J.-B. Leriche, E. Salager, D. Gourier, J.-M. Tarascon and H. Vezin, *Nature Communications*, 2015, **6**, 6276.

17 E. McCalla, A. M. Abakumov, M. Saubanère, D. Foix, E. Berg, G. Rousse, M.-L. Doublet, D. Gonbeau, P. Novak, G. Van Tendeloo, R. Dominko and J.-M. Tarascon, *Submitted to Science*, 2015.

18 M. Sathiya, K. Ramesha, G. Rousse, D. Foix, D. Gonbeau, A. S. Prakash, M. L. Doublet, K. Hemalatha and J.-M. Tarascon, *Chemistry of Materials*, 2013, **25**, 1121–1131.

19 M. Sathiya, A. M. Abakumov, D. Foix, G. Rousse, K. Ramesha, M. Saubanère, M. Doublet, H. Vezin, C. P. Laisa, A. S. Prakash, D. Gonbeau, G. VanTendeloo and J.-M. Tarascon, *Nat Mater*, 2015, **14**, 230–238.

20 J. Rouxel, *Physica B+C*, 1980, **99**, 3–11.

21 L. Blandeau, G. Ouvrard, Y. Calage, R. Brec and J. Rouxel, *Journal of Physics C: Solid State Physics*, 1987, **20**, 42714281.

22 J. Tarascon, G. Vaughan, Y. Chabre, L. Seguin, M. Anne, P. Strobel and G. Amatucci, *Journal of Solid State Chemistry*, 1999, **147**, 410–420.

23 J. Zaanen, G. A. Sawatzky and J. W. Allen, *Physical Review Letters*, 1985, **55**, 418–421.

24 M.-P. Bichat, F. Gillot, L. Monconduit, F. Favier, M. Morcrette, F. Lemoigno and M.-L. Doublet, *Chemistry of Materials*, 2004, **16**, 1002–1013.

25 M.-L. Doublet, F. Lemoigno, F. Gillot and L. Monconduit, *Chemistry of materials*, 2002, **14**, 4126–4133.

26 A. K. Padhi, K. S. Nanjundaswamy, C. Masquelier, S. Okada and J. B. Goodenough, *Journal of The Electrochemical Society*, 1997, **144**, 1609–1613.

27 M. Saubanère, M. B. Yahia, S. Lebègue and M. L. Doublet, *Nature Communications*, 2014, **5**, 5559.

28 A. Van der Ven and G. Ceder, *Electrochemistry Communications*, 2004, **6**, 1045–1050.

29 S. Kim, X. Ma, S. P. Ong and G. Ceder, *Physical Chemistry Chemical Physics*, 2012, **14**, 15571.

30 R. Xiao, H. Li and L. Chen, *Chemistry of Materials*, 2012, **24**, 4242–4251.

31 M. Arroyo y de Dompablo and G. Ceder, *Journal of Power Sources*, 2003, **119-121**, 654–657.

32 A. Jain, G. Hautier, S. P. Ong, S. Dacek and G. Ceder, *Phys. Chem. Chem. Phys.*, 2015, **17**, 5942–5953.

33 N. Yabuuchi, M. Takeuchi, M. Nakayama, H. Shiiba, M. Ogawa, K. Nakayama, T. Ohta, D. Endo, T. Ozaki, T. Inamasu, K. Sato and S. Komaba, *Proceedings of the National Academy of Sciences*, 2015, **112**, 7650–7655.

34 S. Francis Amalraj, B. Markovsky, D. Sharon, M. Talianker, E. Zinigrad, R. Persky, O. Haik, J. Grinblat, J. Lampert, M. Schulz-Dobrick, A. Garsuch, L. Burlaka and D. Aurbach, *Electrochimica Acta*, 2012, **78**, 32–39.

35 S. F. Amalraj, D. Sharon, M. Talianker, C. M. Julien, L. Burlaka, R. Lavi, E. Zhecheva, B. Markovsky, E. Zinigrad, D. Kovacheva, R. Stoyanova and D. Aurbach, *Electrochimica Acta*, 2013, **97**, 259–270.

36 J. Rana, M. Stan, R. Kloepsch, J. Li, G. Schumacher, E. Welter, I. Zizak, J. Banhart and M. Winter, *Advanced Energy Materials*, 2014, **4**,.

37 D. Mohanty, J. Li, D. P. Abraham, A. Huq, E. A. Payzant, D. L. Wood and C. Daniel, *Chemistry of Materials*, 2014, **26**, 6272–6280.

38 E. Canadell, M.-L. Doublet and C. Iung, *Orbital approach to the electronic structure of solids*, Oxford University Press, Oxford ; New York, 2012.

39 R. Dronskowski and P. E. Bloechl, *The Journal of Physical Chemistry*, 1993, **97**, 8617–8624.

40 Z. Lu and J. R. Dahn, *Journal of The Electrochemical Society*, 2002, **149**, A815.

41 A. Armstrong, A. Robertson and P. Bruce, *Journal of Power Sources*, 2005, **146**, 275–280.

42 E. Lee and K. A. Persson, *Advanced Energy Materials*, 2014, **4**,.

43 J.-M. Lim, D. Kim, Y.-G. Lim, M.-S. Park, Y.-J. Kim, M. Cho and K. Cho, *J. Mater. Chem. A*, 2015, **3**, 7066–7076.

44 J. B. Goodenough, *Chemistry of Materials*, 2014, **26**, 820–829.

45 G. Kresse and J. Hafner, *Physical Review B*, 1993, **47**, 558–561.

46 G. Kresse and J. Furthm uller, *Computational Materials Science*, 1996, **6**, 15–50.

47 J. P. Perdew, K. Burke and M. Ernzerhof, *Physical Review Letters*, 1996, **77**, 3865–3868.

48 S. L. Dudarev, G. A. Botton, S. Y. Savrasov, C. J. Humphreys and A. P. Sutton, *Physical Review B*, 1998, **57**, 1505–1509.

49 Y. Miura, Y. Yasui, M. Sato, N. Igawa and K. Kakurai, *Journal of the Physical Society of Japan*, 2007, **76**, 033705.

50 A. Boulineau, L. Croguennec, C. Delmas and F. Weill, *Solid State Ionics*, 2010, **180**, 1652–1659.

51 V. L. Deringer, A. L. Tchougréeff and R. Dronskowski, *The Journal of Physical Chemistry A*, 2011, **115**, 5461–5466.

52 S. Maintz, V. L. Deringer, A. L. Tchougréeff and R. Dronskowski, *Journal of Computational Chemistry*, 2013, **34**, 2557–2567.

V. ACKNOWLEDGEMENTS

A. Author contributions

EMcC and JMT contributed to the general framework of this study by raising the important questions related to the anionic redox in layered transition metal oxides and improved the final manuscript with fruitful discussions. MS and MLD conducted the theoretical framework of this paper, performed the calculations and wrote the manuscript.

Energy & Environmental Science Accepted Manuscript

B.   Additional information

Supplementary information is available in the online version of the paper. Correspondence and requests for materials should be addressed to MLD.

C.   Competing financial interests

The authors declare no competing financial interests.

Broader Context Box

The intriguing $O^{2-}/(O_2)^{(n-)}$ anionic redox at the origin of the extra-capacity measured in Li-rich transition metal oxides is rationalized by means of meaningful Metal-Oxygen bond descriptors and interpreted as a M-driven reductive coupling mechanism. The M-(O_2) covalency is shown to be an absolute condition for the anionic redox to be reversible and to prevent O_2 gas release from the structure at high states of charge, which is crucial application-wise.

A comparative study of the electronic, ionic and structural responses of M(4d)- vs. M(3d)-based $Li_{(2-x)}MO_3$ electrodes upon delithiation provides a clear picture of how each system dynamically responds to the creation of unstable holes on the oxygen network, leading to either a classical reversible cationic redox, an original reversible anionic redox or a damaging irreversible anionic redox. This analysis provide new perspectives in controlling the oxygen redox activity in high-capacity electrodes materials.